Solution-processed flexible n-type S-doped Ag2Se thermoelectric generators for near-ambient-temperature energy harvest†

Chenghao Xin, Zhuoqun Fang, Shan Jiang, Zhelu Hu, Dongjiu Zhang, Francis Cassagne, Lionel Aigouy, Zhuoying Chen

Materials Today Energy 33 (2023) 1012

https://doi.org/10.1016/j.mtener.2023.101266

Solution-processed flexible n-type S-doped Ag2Se thermoelectric generators for near-ambient-temperature energy harvest

Chenghao Xin, Zhuoqun Fang, Shan Jiang, Zhelu Hu, Dongjiu Zhang,

*Francis Cassagne, Lionel Aigouy, Zhuoying Chen**

Corresponding author. E-mail address: zhuoying.chen@espci.fr

Abstract:

Among the different technologies to harvest renewable energy, thermoelectric (TE) generators (TEGs) represent a highly promising route capable of converting heat to electricity based on the Seebeck effect. Here, a new room temperature (RT) one-pot solution synthesis approach was proposed, together with a sulfur-doping strategy, to optimize the flexibility and the power factor of n-type S-doped Ag_2Se TE thin films deposited by solution-processes, requiring only mild post-deposition annealing at 150°C. Optimized S-doped flexible Ag_2Se thin films exhibited a maximum power factor of ~2058 μW/m/K^2 at RT, allowing for the fabrication of flexible TEGs with a maximum power output (Pmax) of 3.98 μW under a near-RT ΔT of 31 K, equivalent to a power density of 11.06 W/m^2 . Multidomain applications were further demonstrated by these heavy-metal-free, flexible TEGs to harvest near-RT waste heat from laptop computers, non-concentrated sun light, and human body together with the realization of a self-powered motion detector. The current findings open promising paths for innovations on low-cost wearable smart electronics and energy harvesting.

Keywords:

Solution-processed, Thermoelectrics, Thermoelectric energy conversion, Low-grade heat, Heat harvesting, Nanotechnology

1. Introduction

Facing the ever-rising energy demand worldwide, we urgently need to increase our energy production from renewable and sustainable sources. Among the different technologies to harvest renewable energy, thermoelectric (TE) generators (TEGs) represent a highly promising route capable of converting heat to electricity based on the Seebeck effect [1-4], through which a voltage can be generated between the cold and hot ends of a TE material. In particular, there exist abundant, ambient and near-room temperature (near-RT) low-grade waste heat sources, such as those from human body, household electronics, and sun illumination. At the arrival of the internet-of-things era, the research to identify new routes to efficiently harvest near-RT heat sources into energy in an ideally flexible and wearable manner is of high importance to develop next-generation consumable electronics and to reduce our dependence on non-renewable energy sources [5-11].

Under this context, much research effort has been focused recently on the quest of flexible, solution-processed, and lowtemperature-derived material alternatives for near-RT TE applications [3,7,11-14]. So far, promising TE functionality together with flexibility has been observed on conductive polymers [3], carbon nanotubes (CNTs) and their hybrid composites [12,13], and a few families of inorganic semiconductors, where processing in form of a powder-formulated ink is possible [15-21]. For a given TE material, its energy conversion efficiency can be evaluated by a dimensionless figure-of-merit defined as $ZT = S^2\sigma T/k$, where S, σ, k, and T are the Seebeck coefficient, electrical conductivity, thermal conductivity, and absolute temperature, respectively. *ZT* is governed, simultaneously, by both the material's electrical property, represented by the power factor (*PF*, defined as $S^2\sigma$) and thermal property, represented by the thermal conductivity k. For conductive polymers, despite the intrinsic advantages in terms of low thermal conductivity, their low Seebeck coefficients lead to only a modest PF, typically ranging from a few tens to a few hundreds of $\mu W/m/K^2$ and a maximum *ZT* of 0.42 [22-25], with the exception of p-type electrochemically-reduced poly (3,4-ethylenedioxythiophene) (PEDOT) films on which a maximum RT *PF* of 1270 $\mu W/m/K^2$ was reported under an external applied voltage [26]. In addition, the *PF* demonstrated on n-type polymers remains more than an order of magnitude smaller than those of p-type polymers [27]. The formation of CNT/polymer composites allows for the freedom to engineer p- or n-type conductivity of the final organic composite, resulting in reported *PF*s of a similar order of magnitude as those obtained in conductive polymers [28]. Nevertheless, the synthesis of CNTs is energy demanding, typically requiring chemical vapor deposition-based processes and a high deposition temperature (~1000 °C or more) [29]. On inorganic semiconductor thin films, p-type $Bi_{0.4}Sb_{1.6}Te_3$ thin films screen-printed from a ball-milled nanoparticle ink demonstrated an impressive *PF* of about 3000 $\mu W/m/K^2$ at RT and *ZT* of about 1 [15]. Yet, the relatively high post-printing sintering temperature (at 450 °C) of these $Bi_{0.4}Sb_{1.6}Te_3$ thin films is not compatible to common polyethylene terephthalate (PET) and polyethylene naphthalate flexible substrates. By comparison to the above-mentioned materials, the inorganic silver chalcogenides Ag_2X (X = S, Se, or Te) is currently considered as one of the most promising material families for flexible TE application near-RT [7,30-34]. In particular, bulk α-Ag_2S (monoclinic, RT phase [35]) has been recently discovered as one of the rare inorganic semiconductors exhibiting surprising metal-like ductility [33]. But its poor TE property near RT hinders its further application [16,33]. In contrast, bulk α-Ag_2Te (monoclinic at RT) and β-Ag_2Se (orthorhombic at RT) are not ductile but they exhibited much better TE characteristics, in view of their higher near-RT *PF* (~2000 $\mu W/m/K^2$ for bulk Ag_2Te and ~3500 $\mu W/m/K^2$ for bulk Ag_2Se) and *ZT* (~0.5 for Ag_2Te and ~1 for Ag_2Se) from previous reports [30-32]. The RT *ZT* of n-type β-Ag_2Se has recently been further boosted to 1.2 by pulsed hybrid reactive magnetron sputtering [34]. In order to tailor both the TE characteristics and mechanical flexibility, the formation of alloys by doping S into bulk Ag_2Se and Ag_2Te was found to be a promising approach [7,16]. For example, very recently, highperformance p-type ductile TE materials were discovered on AgCu(Se, S, Te) pseudo-ternary solid solutions, exhibiting a *ZT* of 0.45 at 300 K and 0.68 at 340 K [7]. Nevertheless, prolonged hightemperature annealing at 1323 K is required to obtain these alloy TE materials. In addition to S-doping, various other attempts have been made to obtain TE thin films, which can lead to flexible Ag_2X (X = Se or Te) TEGs. For example, flexible Ag_2X TE thin films have been reported by 'top-down' methods involving a conventional high-temperature synthesis (at > 1000 °C) and a subsequent crushing or cutting of ingots

together with hot-pressing into flexible thin films [16,17]. By the technique of hot-pressing, which typically requires a few MPa of pressure and a simultaneous heattreatment, various 'bottom-up' synthesized nano- and sub-micron size Ag_2Se powers were integrated into flexible TE thin films [18-20]. Recently, without the use of any vacuum equipment, high-temperature annealing, or hot-pressing, Lemmer et al. reported an one-pot solution synthesis of the Ag_2Se ink formulated with the aid of a commercial additive [36], of which the exact type and composition remain nevertheless obscure. The screen printing of this ink generated flexible Ag_2Se TE thin films, requiring a postdeposition temperature as low as 200 °C, with a maximum PF of about 1700 μW/m/K^2 and ZT of 1.03 at 300 K [36]. By coupling these n-type Ag_2Se thin films together with p-type PEDOT:PSS legs, flexible TEGs were demonstrated on polyethylene naphthalate substrates, exhibiting a maximum power output (Pmax) of 0.19 μW under a temperature difference (ΔT) of 75 K [36].

In this work, we propose a new RT one-pot solution synthesis approach for the Ag_2Se ink, which can be solution processed into flexible n-type TE thin films requiring only a post-deposition heat treatment at a mild temperature as low as 150 °C. By applying sulfur-doping (S-doped) directly into the Ag_2Se ink synthesis, both the flexibility and the TE characteristics of the achieved thin films are optimized, with the best sample exhibiting a maximum PF of ~2058 μW/m/K^2 at RT. These flexible n-type S-doped Ag_2Se thin films are further integrated into functional and flexible TEGs under both the uni-leg and p-n (by coupling with p-type PEDOT:PSS) configurations, with the optimized TEG exhibiting a maximum power output Pmax of 4.2 μW under a near-ambient ΔT of 31 K. We further show that these flexible TEGs can perform near-RT energy harvest from various low-grade heat sources including laptop computers, non-concentrated sun light, and human body, together with the demonstration of TEG-enabled self-powered human motion detection.

Table 1
The atomic percentage detected and the equivalent composition of the achieved thermoelectric thin films determined by Energy-dispersive X-ray spectroscopy spectroscopy from different spots of the same sample.

	Composition determined by Energy-dispersive X-ray spectroscopy on thin films	
	Ag/Se/S (atomic %)	Equivalent composition $Ag_xSe_yS_z$
Undoped	67.66 ± 0.90/32.67 ± 0.43/0	$Ag_2Se_{0.966}$
Sample A	65.95 ± 0.61/33.19 ± 0.61/0.86 ± 0.15	$Ag_2Se_{1.007}S_{0.026}$
Sample B	65.30 ± 0.31/33.05 ± 0.39/1.65 ± 0.17	$Ag_2Se_{1.012}S_{0.050}$
Sample C	64.31 ± 0.67/33.56 ± 0.73/2.13 ± 0.14	$Ag_2Se_{1.044}S_{0.066}$
Sample D	61.81 ± 0.56/33.23 ± 1.18/4.90 ± 0.56	$Ag_2Se_{1.075}S_{0.159}$

2. Experimental details

2.1. Materials

Se powder (100 mesh, 99.5%), Ag powder (2-3.5 mm, ≥99.9%), S powder (≥99.9%), polystyrene (average Mw = 192,000 g/mol), toluene (anhydrous, ≥99.8%), PET (Polyethylene terephthalate) flexible substrates (thickness = 175 μm), CuSe (≥ 99.5%), a CNT (a single-walled, solvent-based conductive ink, SWCNT), ethyl cellulose (viscosity 10 cP and 46 cP, 5% in toluene/ethanol 80:20 (lit.)), ethylene glycol (99.8%), α-terpineol (90%), and titanium isopropoxide were obtained from Sigma Aldrich/Merck. PEDOT:PSS (PH1000) was purchased from Ossila. Conductive silver paint (no. 123-9911) and conductive carbon paint (no. 835-2699) were obtained from RS Components.

2.1.1. Synthesis & deposition for different undoped and S-doped Ag_2Se thin films

Briefly, for the undoped Ag_2Se ink, 0.305 g (2.8 mmol) of Ag and 0.11 g (1.4 mmol) of Se powders were mixed in 0.4 mL toluene together with 0.025 g of polystyrene. For the S-doped inks, in addition to the above-mentioned materials and solvents, various amounts of sulfur powders (0.005 g, 0.01 g, 0.015 g, and 0.025 g, corresponding to 0.156 mmol, 0.312 mmol, 0.468 mmol, and 0.780 mmol, respectively) were added in order to achieve different levels of S-doping in sample A, B, C, and D, respectively. This was followed by an addition of 50 μL of an adhesive solution, which was pre-formulated by string 0.1 g of ethyl cellulose (10 cP), 0.1 g of ethyl cellulose (46 cP), 8 ml of α-

terpineol, and 0.5 ml of titanium isopropoxide together at RT until forming a homogenous solution. This solution was then stirred for at least 72 h at 1200 rpm at RT leading to the formation of a dark-color ink. Any un-dissolved precipitate found at the bottom of the ink container was discarded before the ink was applied for the fabrication of the TE legs. We found that the addition of the adhesive solution was necessary to form the Ag_2Se ink. As shown in Fig. S1 of the supporting information, without the adhesive addition, even under prolonged stirring and sonication, it is not possible to obtain a semi-stable Ag_2Se ink for the thin film deposition. To form undoped and S-doped Ag_2Se legs on substrates, the ink was printed by a doctor blading through a screen mask onto the unmasked areas of the PET substrates followed by drying on a hotplate at 150 °C in air for 10 min prior to mask removal. Each thin film Ag_2Se leg (to build the undermentioned TEGs) has a geometrical dimension of about 3 mm (width) × 15 mm (length) × 10 mm (thickness). The synthesis and deposition procedures for different p-type flexible thin films are described in the supplementary material.

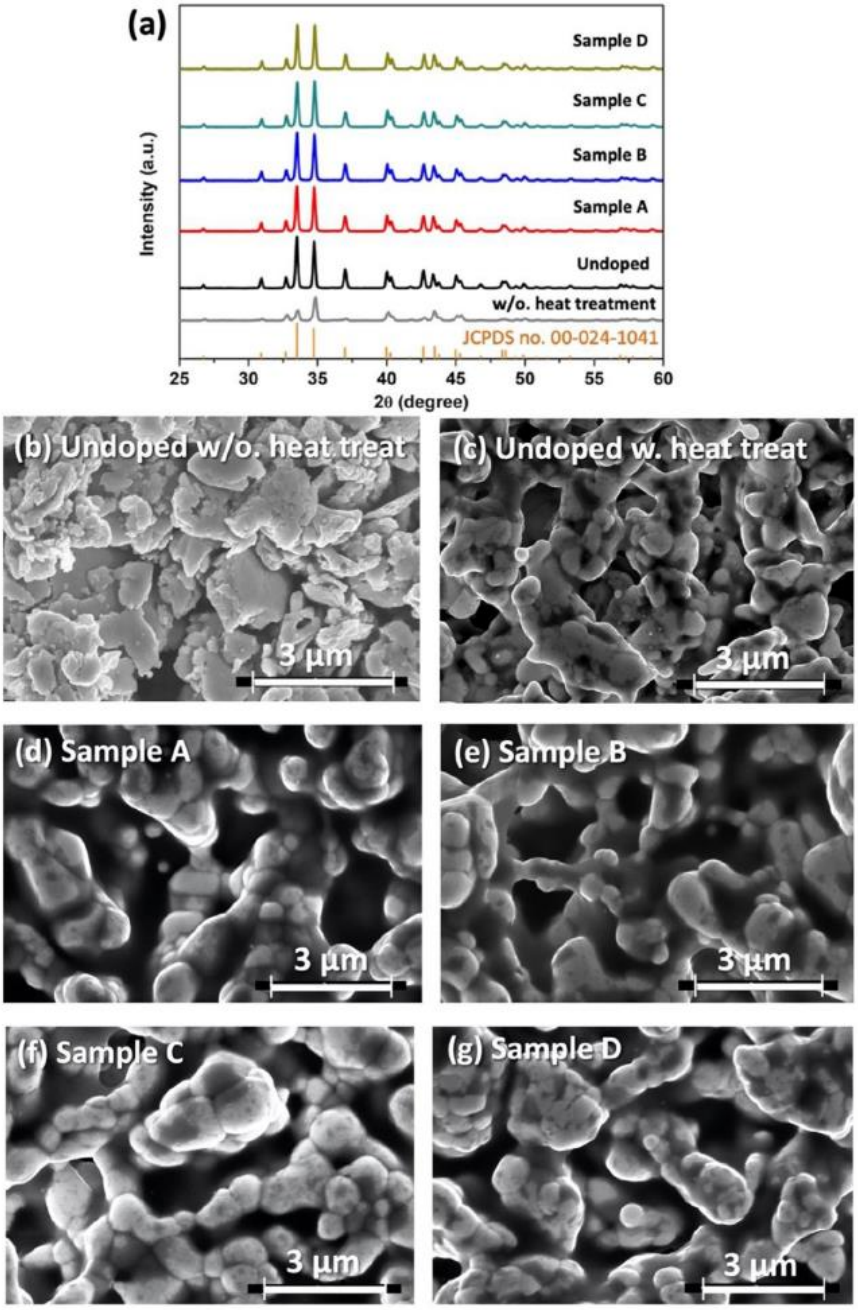

Fig. 1. X-ray diffraction spectra (a) and SEM images (b-g) of the different thermoelectric thin films under study. The compositions of undoped and S-doped samples are listed in Table 1. (c)-(f) were measured on samples after a 150 °C post-deposition heat treatment.

2.1.2. Fabrication of p/n- and uni-leg-type TEGs

Upon defining the legs by the above-mentioned procedures, gold electrodes were evaporated through a shadow mask by thermal evaporation (with a chamber pressure connection between the p- and n-legs was achieved by the abovementioned gold electrodes. For the uni-leg-type TEGs, after evaporating gold electrodes on the two ends of each leg, they were further connected to each other (with hot ends connected to cold ends) by silver lines achieved by commercial silver paint. Care was taken to not avoid direct contact between the Ag_2Se legs and the silver paint. In the case of contact issues, conductive carbon paint was applied between the silver lines and the evaporated gold electrodes.

2.2. Characterizations

The thin film thickness was measured by a Dektak mechanical profilometer. Scanning electron microscopy (SEM) and Energydispersive X-ray spectroscopy (EDX) characterizations were performed by a FEI Magellan 400 system with a standard field emission gun source and equipped with EDX. X-ray diffraction (XRD) spectra were measured by a PANalytical X'Pert X-ray diffractometer using Cu-Kα radiation. X-ray photoelectron spectroscopy (Thermo ESCA-LAB 250 Xi), using Al-Kα radiation, was used to examine the binding energies of the elements of the undoped and different S-doped Ag_2Se samples.

To cross-compare the PF of different TE thin films under study, their RT electrical conductivities were measured in air by a standard four-point probe method (by an Ossila Four-Point Probe system with a built-in source measurement unit). Their RT Seebeck coefficients were measured and cross-compared in an argon-filled glovebox by a home-built setup according to previously reported methods [37,38], while a commercial physical property measurement system (PPMS, Quantum Design) system was applied on the most optimized thin film sample to determine its Seebeck coefficient at different temperatures and to perform Hall effect measurements with an applied reversible magnetic field up to ± 3T allowing (to determine the sample's electrical conductivity (σ), carrier type, carrier mobility (μ), and carrier density (n) at a certain temperature). For the measurement of the temperature-dependent Seebeck coefficient, the sample was fixed onto a PPMS puck with the cold end contacting a copper heat-sink stage and the hot end contacting a current-controlled heating table (by a chip-fixed resistor of 1000 Ω). Two Pt100 temperature sensors were fixed onto the two ends of the sample to measure the temperature difference obtained, and the Seebeck coefficient was measured by recording the Seebeck voltage (ΔV) induced by temperature gradient (ΔT).

To characterize the achieved TEGs, a dual-channel Keithley 2632 SMU was applied to measure the current-voltage characteristics of the device under test at a fixed ΔT achieved between the hot and cold end of the sample. In such a measurement, one SMU (SMUA) was applied as a current source I (acting a similar function as a variable load resistance R_L) while the other SMU (SMUB) was applied as a voltmeter to measure the output voltage (V) between the two ends of the device. The generated power from the TEG can be obtained by $P = I \cdot V = I^2 R_L = [V_{oc} / (R_{int}+R_L)]^2 \cdot R_L$ [39], where the R_{int} is the internal resistance of the TEG and V_{oc} is the open-circuit voltage. The different ΔT was created between the hot and cold ends of the sample by placing the hot end onto a temperaturecontrolled hot-plate. The achieved ΔT was further monitored by two external digital thermometers (RS PRO RS42).

For the demonstration of solar energy harvest, a photothermal coating based on plasmonic gold nanoparticle (NP) were applied on the hot end of the TEG, as described in our previous work [40]. This photothermal coating converts the absorbed solar illumination into heat. The half-hidden (with the cold end hidden from illumination) TEG was then placed under a class AAB (ASTM) ABET solar simulator (with an AM 1.5G filter) operated at 1-SUN (100 mW/ cm^2) at an ambient condition. The output voltage was measured by a digital multimeter. For the demonstration of self-powered human motion detection: the hot-end of the TEG under test was hand-held (i.e. in-contact with a human palm) while the cold-end was left in ambient air. A ΔT was created by the temperature difference between the hand and the ambient temperature. A circuit is made so that the output of the TEG was connected to two resistors in series so that the output voltage of the TEG was shared between these two resistors (described below in section

3.4), among which one (R_1) is a fixed-value resistor (R_1 = 1.19 ± 0.05 MΩ) and R_f is a force sensing resistor (FSR03BE from OHMITE). This force sensing resistor Rf was then attached onto a human arm by a medical adhesive tape. During the repetitive arm movements, the evolution of the voltage felt onto R_1 over time was monitored by a computer-controlled Keithley 2632B SMU.

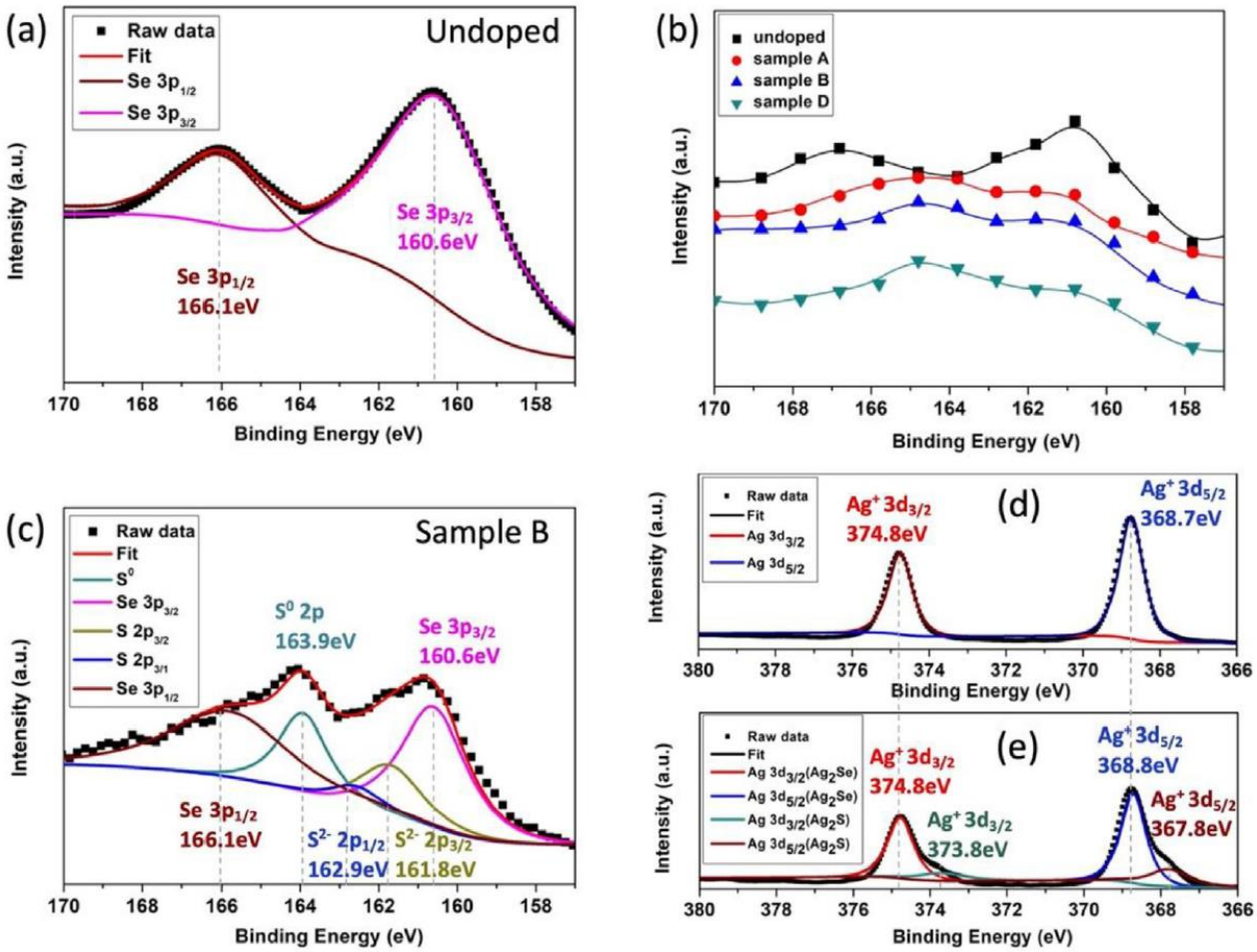

Fig. 2. (a) An X-ray photoelectron spectroscopy (XPS) spectrum of the Se 3p regions of an undoped Ag_2Se thin film; (b) The evolution of the XPS spectra in the same spectral region comparing an undoped and different S-doped Ag_2Se thin films. (c) An XPS spectrum of the Se 3p and S 3p regions a doped sample B. (d) and (e) XPS spectra of the Ag 3p regions of an undoped (d) and doped sample B (e).

3. Results and discussion

3.1. Undoped and S-doped Ag_2Se ink and their n-type TE thin films

Various extents of sulfur doping were achieved by applying different amounts of sulfur powders directly into the reactants for ink formation (c.f. Experimental details). Table 1 lists the molar percentage of the different elements measured on the achieved TE thin films by EDX spectroscopy (coupled with SEM), averaged from different spots of each sample and the corresponding equivalent composition. EDX elemental mapping together with SEM imaging is shown in Fig. S2 of the supporting information. EDX results revealed that the undoped sample was slightly Se-deficient or Agexcess (with an average Ag/Se molar ratio slightly >2:1). Ag excess may not be advantageous for the thin film's TE property due to the possible formation of metallic clusters. With the addition of sulfur doping, this situation is progressively inversed, resulting in slight Se excess as the S-doping increases. Sample A, the sample with the smallest amount of S-doing, exhibits an average Ag/Se molar ratio very close to 2:1 (Table 1, results are averaged on five different spots of the same sample). Nevertheless, for sample A, on some sample spots, Se-deficient or Ag-excess was still detected (e.g. two out of five sample spots still exhibiting a Ag/Se ratio >2:1, Table S1). With a further

increase of S-doping likely providing sufficient anions to react with all available or excess Agþ cations, on sample B, C, and D, all examined sample spots exhibit an Ag/Se ratio close to 2:1 (sample B) or < 2:1 as S-doping further increases (sample C and D).

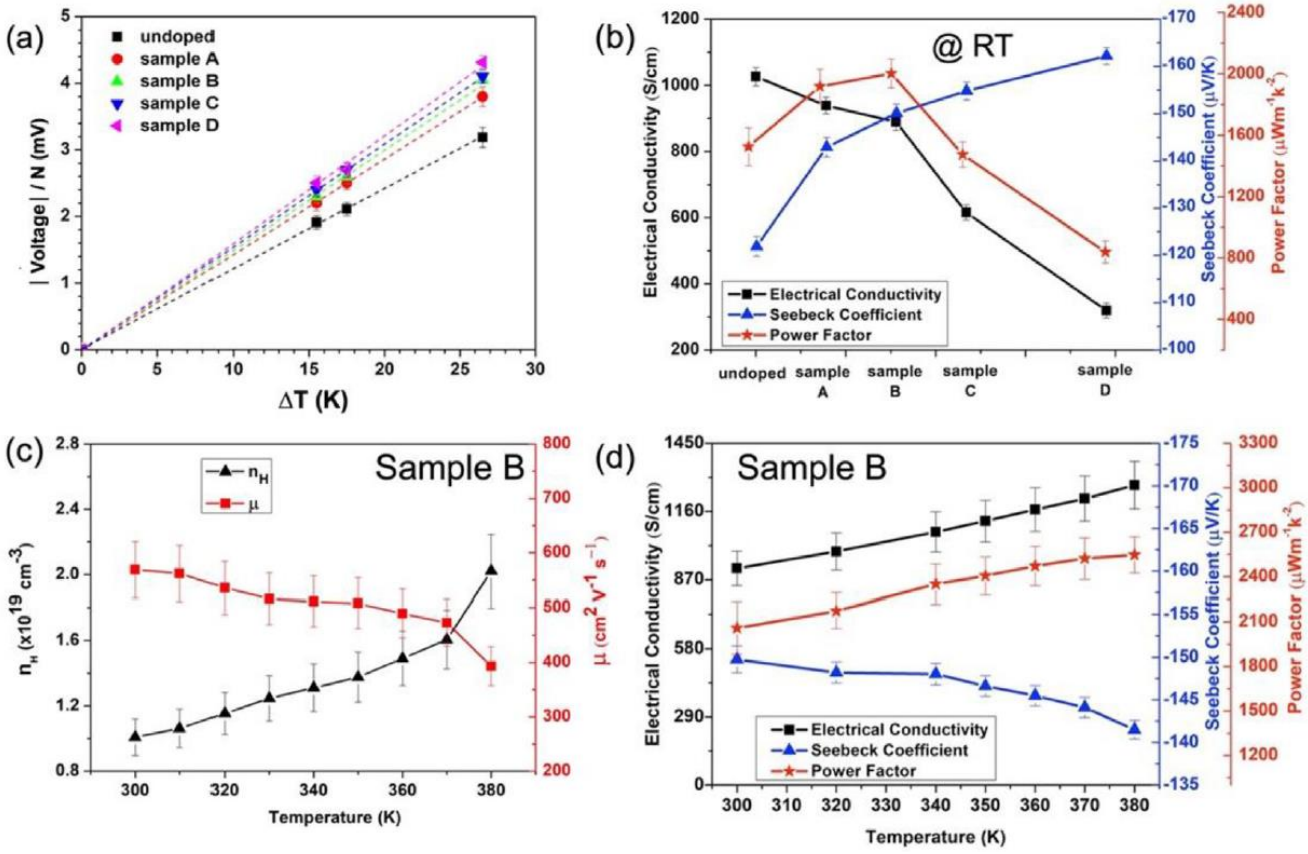

Fig. 3. (a) and (b): Cross-comparison of the thermoelectric properties of different undoped and S-doped Ag2Se thin film samples under study. (a) The absolute value of the Seebeck voltage per leg, measured on eight legs of each sample connected in series, over different DT measured between the hot and cold electrodes; (b) The room temperature electrical conductivity, Seebeck coefficient, and power factor values of samples with different S-doping. (c) and (d): On the optimized doping condition (sample B), the temperature dependence of (c) carrier concentration (n) and Hall mobility (m) as well as (d) electrical conductivity, Seebeck coefficient, and power factor were measured for the near-room temperature range from 300 to 380 K.

All TE thin films under study exhibited a phase-pure orthorhombic b-Ag_2Se phase (JCPDS no. 00-024-1041) revealed by XRD (Fig. 1(a)), without the appearance of any diffraction peaks corresponding to the elemental S, Ag_2S, or Ag phase. It is likely that the amounts of these impurity phases, if existed in some samples, were too little to be identified in XRD experiments. The mild postdeposition heat treatment at 150 °C significantly enhances the thin film's crystallinity (Fig. 1(a), grey and black curve), resulting in stronger and narrower diffraction peaks. From the Debyee-Scherrer formula, an average grain size of the heat-treated thin film is estimated to be about 40 nm, while by the same method, the average grain size of the film before heat treatment is only about 28 nm. Besides the enlarged grain size, from SEM measurements (Fig. 1(b) and (c)), we observe that, after the heat treatment, the different multicrystalline domains are fused together, forming interconnected networks with smooth edges, which is likely favorable for charge transport properties. This is further confirmed by the increase of electrical conductivity (s) found on the heat-treated Ag_2Se thin films ($\sigma = 1026 \pm 40$ S/cm) compared to the non-heat-treated films ($\sigma = 125 \pm 1$ S/cm) (Fig. S3). Concerning the undoped and S-doped Ag_2Se thin films after the heat treatment (Fig. 1(c)-1(g)), SEM revealed similar morphologies, with interconnected domains formed by multiple crystalline grains and with a slight coarsening of these domains as the extent of S-doping increases (Fig. S4 of supporting information). X-ray photoelectron spectroscopy was applied to examine the surface chemistry of the undoped and S-doped Ag_2Se thin films (Fig. 2). For the undoped thin film, one can observe that the Se 3p core splits into a doublet of Se $3p_{3/2}$ and Se

$3p_{1/2}$ at binding energies of ~160.6 eV and ~166.1 eV, respectively (Fig. 2(a)), together with the identification of Ag $3d_{5/2}$ at ~368.7 eV and Ag $3d_{3/2}$ at ~374.8 eV (Fig. 2(d)). The binding energies and the shapes of these Se 3p and Ag 3d peaks are consistent with Se^{2-} and Ag^{+} in a Ag_2Se lattice [41-43]. Upon S-doping, a clear peak-shape modification can be observed at the binding energies corresponding to the doublet of Se $3p_{3/2}$ and Se $3p_{1/2}$ (Fig. 2(b)), with fittings revealing a major contribution from S^0 2p (163.9 eV), as well as some minor contributions from S $2p_{3/2}$ (~161.8 eV) and S 2p1/2 (~162.9 eV), suggesting sulfur exists on the surface of the thin film mainly as S^0 together with some minor contribution of Ag_2S [42,44]. This corroborates with the formation of peak shoulders on the Ag $3d_{5/2}$ and Ag $3d_{3/2}$ peaks upon S-doping (Fig. 2(e)) due to the slightly lower binding energies of the Ag 3d peaks in Ag_2S compared to those in Ag_2Se [45].

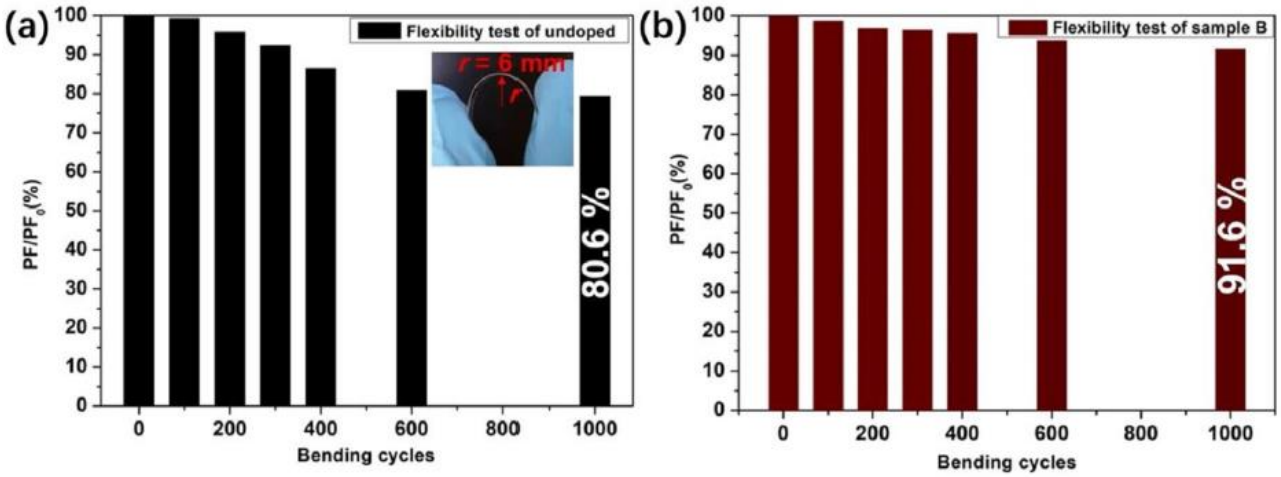

Fig. 4. Bending tests comparing the power factor loss over initial values of an undoped (a) and S-doped (b) Ag_2Se thin film on a polyethylene terephthalate substrate with a bending radius r = 6 mm. Inset shows the sample image under bending.

3.2. TE properties and flexibility

The TE properties of the undoped, different S-doped Ag_2Se and various p-type flexible thin films were first cross-compared by examining their electrical conductivity, Seebeck coefficient, and *PF* at ~RT. For such a cross-comparison, for a given sample, 'uni-leg'- type devices were fabricated on PET substrates, where a few numbers (N) of thin film stripes were connected in series (N ¼ 8 legs for Ag2Se devices). The near-RT Seebeck coefficient ($\Delta T \leq$ 26.5 K) was then estimated by the slope of the linear fit of the Seebeck voltage (ΔV) normalized per leg generated under different steady temperature differences (ΔT) between hot and cold ends, as in methods reported previously [29,37,38]. On n-type undoped and S-doped Ag2Se thin films, results indicate that at ~RT the thin film's conductivity progressively decreases while its Seebeck coefficient slightly increases along with the addition of S-doping (Fig. 3(a) and (b)). This corroborates with the above-presented EDX results as in the undoped and sample A (i.e. the smallest amount of S-doping) Ag excess was found in all or some sample spots. The excessive silver may lead to the formation of metallic clusters favorable to conductivity but not to the sample's Seebeck coefficient [34,36]. As shown in Fig. 3(b), a maximum PF reaching 2003 $\mu W/m/K^2$ at RT was obtained on sample B with a mild S-doping. This doping condition will thus be chosen as the optimized condition for the following experiments and discussions. The results obtained on different p-type materials are summarized in the supplementary information (Fig. S5).

The temperature-dependent TE property of the optimized sample B was further characterized by a PPMS system (Fig. 3(c) and (d)). By PPMS, Hall effect measurements were performed on the sample, revealing a negative Seebeck coefficient confirming that the conductivity is n-type. For the near-RT temperature range (300-380 K), the main temperature window targeted by near-RT energy harvest, as temperature increases, the Hall mobility, and the absolute value of the Seebeck coefficient were found to slightly decrease while the carrier density and conductivity slightly increased. The PF remains overall stable over this temperature range, with *PF* = 2058 ± 177 $\mu W/m/K^2$ measured at 300 K and *PF* = 2547 ± 122 $\mu W/m/K^2$ measured at 380 K. Previously, on offstoichiometric solution-

processed $Ag_{2\pm x}Se$ thin films achieved by an annealing temperature of 200 °C [36], a maximum *PF* of ~1700 μW/m/K^2 could be obtained at RT. The *PF* values obtained in the current S-doped Ag_2Se thin films at RT are therefore remarkable, especially considering the facile RT solution-synthesis and the very low-heat treatment temperature (150 °C) required in the present work.

Besides the optimization in terms of the above-mentioned TE characteristics, S-doping was also found to enhance the flexibility of the doped Ag_2Se thin films. A bending test was performed to compare the undoped Ag_2Se thin film and S-doped Ag_2Se thin film (Sample B condition), both of which were deposited on a PET substrate. The sample under study was applied around a rod with a radius of 6 mm, while its RT electrical conductivity and Seebeck coefficient were monitored over different numbers of bending cycles. As shown in Fig. 4, after 1000 cycles of bending, sample B maintained >91% of its initial *PF*, while for the same condition, the undoped sample exhibited only ~81% of its initial *PF*. From the evolution of the conductivity and Seebeck coefficient over bending cycles (Fig. S6), we observed that, upon 1000 cycles of bending, on the undoped sample, there was a ~9% loss in terms of conductivity and a ~6% loss of Seebeck coefficient. This was improved on the Sdoped sample B, where only a 6% decrease in terms of conductivity and a 1% decrease of Seebeck coefficient were observed after 1000 bending cycles. The origins leading to the improved flexibility due to S-doping in the current samples are still to be debated. While we cannot exclude the role of the more ductile nature of Ag_2S [33], it is likely not the major reason leading to the flexibility improvement due to the minor amount of S-doping in the current samples (Table 1). Nevertheless, a change of the thin film morphology can be observed due to S-doping (Fig. 1 and Fig. S7). By comparing the lowmagnification SEM images of the undoped and S-doped sample (Fig. S7), we observed a more porous (and less compact) morphology in the doped films. As porous structures have been previously found to favor the mechanical flexibility of thin films [18,46], the S-doping-induced change in the film morphology likely plays a major role here, contributing to the observed improved flexibility.

3.3. TEGs by S-doped Ag_2Se thin films

To demonstrate the energy-harvesting functionality, flexible TEGs were fabricated by applying the optimized S-doped Ag_2Se TE thin films (sample B condition) with a film thickness of ~10 μm under both an uni-leg (Fig. 5(d)-(e)) and a p/n-type (Fig. S8) device architecture on a PET substrate. Fig. 5(a) and (b) shows the measured current-voltage (*I*-*V*) and power-load resistance (*P*-R_L) characteristics of the optimized TEG at different ΔT near RT. Similar characteristics of a p-n type TEG applying the optimized S-doped Ag_2Se legs together with p-type PEDOT:PSS legs are shown in the supporting information (Fig. S8). Here, in Fig. 5, the uni-leg TEG allows for a higher power output as compared to the p-n type TEG due to the large PF differences between n and p-type legs (Fig. 3(b) and Fig. S5). On an optimized uni-leg TEG, a maximum output (*P*) was found when the load resistance RL equals to ~ 176 U, below referred as $R_{L,Pmax}$. From the relationship between $R_{L,Pmax}$ and the value of the internal resistance (R_{int}) in TEGs, $R_{L,Pmax} = R_{int}(1+ZT)^{1/2}$ [47,48], we estimate that the R_{int} of the current device should be within the same order of magnitude but slightly smaller than 176 Ω.

While the present internal resistance value is much larger than some previous works [20], it is still within a reasonable range when comparing with the values reported in other studies [18,49]. For example, by a similar uni-leg TEG device structure applying n-type Ag_2Se thin films, Ding et al. [18] reported an internal resistance of 250 Ω. Lu et al. [49] reported an internal resistance of about 150 Ω on uni-leg TEG devices applying Ag_2Se/Ag/CuAgSe composite thin films. Here, R_{int} should be composed of three parts: the total resistance (R_a) of the 12 TE legs, the resistance of the silver lines (R_b, formed by silver paint), and the contact resistance (R_c) between the TE legs and the gold electrodes. By applying the RT conductivity of the TE legs (Fig. 3(d)) and their geometrical dimensions, R_a can be estimated to be ~ 70 Ω. To a first approximation, R_b is ignored due to the highly conductive silver paint applied (with a typical sheet resistance in the order of a few tens of mΩ/square). Based on a rough approximation of $R_{int} \approx R_{L,Pmax}$ = 176 Ω, which somehow overestimates the value of R_{int}, we can further estimate the contact resistance ($R_c \approx R_{int} - R_a$) to be about 100 Ω in total or about 8 Ω per leg. We note that a nearly ohmic contact between gold electrodes and

hot-pressed Ag_2Se films was achieved previously [20]. In comparison, the reason behinds such a relatively large contact resistance in the current study may be attributed to a slight overestimation of R_{int}, the organic-inorganic hybrid nature of the current S-doped Ag_2Se thin films as well as their porous morphologies. Indeed, additional contact barriers between the legs and the electrode can result from the organic materials (e.g. polystyrene and the adhesive solution added into the ink formulation) remained in the film.

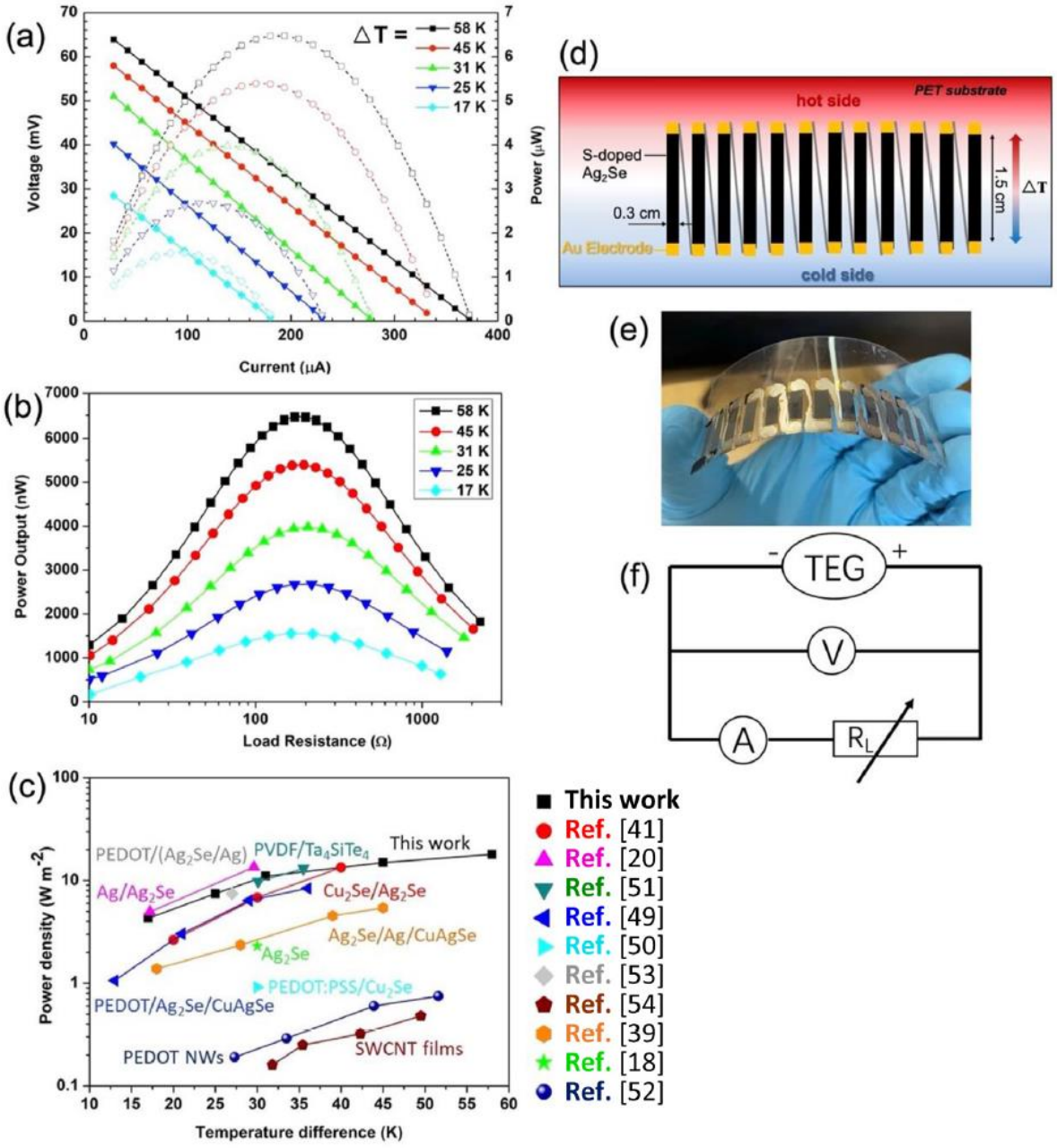

Fig. 5. Steady-state (a) current-voltage (I-V) and (b) power output-load resistance (P-R_L) characteristics curves measured under different ΔT on an uni-leg-type thermoelectric generator (TEG) formed by 12 legs of S-doped Ag_2Se (sample B doping condition) on a polyethylene terephthalate substrate. (c) The comparison between the maximum power density generated by the current S-doped Ag_2Se TEG and those reported in the literature. (d)-(e) Schematic (d) and optical image (e) of the S-doped Ag_2Se TEG under study. (f) Schematic of the equivalent circuit applied to characterize the TEG under study.

Remarkably, a maximum power output reaching ~1.55 μW, 2.68 μW, 3.98 μW, 5.39 μW, and 6.47 μW was measured, corresponding to a different near-ambient ΔT of ~17 K, 25 K, 31 K, 45 K, and 58 K, respectively. Dividing the maximum output P by the sum of the cross-sectional area (A) of all legs, the maximum power density (defined as $P_{density} = P/(A \cdot N)$, where N is the number of legs) [20] achieved by the current TEG can be obtained and plotted in Fig. 5(c) over different ΔT, together with other results from the literature for comparison. For example, under a ΔT of ~30

K, which was considered as a most relevant ΔT for near-RT energy harvest [8,50,51], a power density of 11.06 W/m^2 was achieved by the current optimized S-doped Ag_2Se TEG. This value is significantly higher than those obtained on previous TEGs based on PEDOT [49,50,52,53], CNTs [54], silver and/or copper chalcogenides [18,41,49,50], and their composites [39,53]. Indeed, the current $P_{density}$ value at ΔT = ~30 K is only slightly lower (but remains comparable) to that reported on TEGs based on Ag/Ag_2Se nanodendritic composite powders [20], where a maximum $P_{density}$ of 13.56 W/m^2 was reported at ΔT = 30 K. But these previous nanodendritic composite samples were not solution-processed (i.e. requiring hot pressing at 210 °C and 1 MPa). The current flexible TEGs, employing RT solution synthesis/processing and requiring only a mild post-deposition heat treatment at 150 °C, thus represent a significant progress towards the large-scale development of this technology.

3.4. Application of S-doped Ag_2SeTEGs on near-RT energy harvesting

We further demonstrate that the optimized S-doped Ag_2Se TE flexible thin films proposed in this work can be applied into various situations to perform near-RT low-grade heat harvesting (Fig. 6), suggesting bright perspectives for their applications in future wearable self-powered smart electronics [55]. For example, the temperature difference between a laptop running at its full potential and an ambient condition (e.g. at ~25 °C) can reach ~10 K. Under this situation, by fixing the hot end of the above-mentioned uni-leg-type S-doped Ag_2Se TEG onto the laptop, an open-circuit output voltage of ~10 mV can be obtained (Fig. 6(a)). In terms of solar light harvest, here, we applied onto the hot end of the current S-doped Ag_2Se TEG the same plasmonic Au NP photothermal coating as the one proposed in our previous work [40]. Such a plasmonic photothermal coating absorbs the visible part of the non-concentrated sun illumination and converts the absorbed light into heat, generating a ΔT ~40 K between the hot and the cold end of the device. As a result, even though the current sun illumination spot only covers 58% of the hot end area (i.e. covering 7 legs out of 12 legs), an open-circuit output voltage reaching ~32 mV can already be obtained by the current TEG (Fig. 6(b)). Estimated from the *I-V-P* characteristics shown in Fig. 5(a), under a ΔT of ~40 K, if achievable thanks to sunlight and the photothermal coating, a maximum output P_{max} of ~4.6 μW can be obtained by the present TEG. This is significantly larger than the value reported in our previous study (P_{max} ~ 146 nW at ΔT ~ 40 K) [40] due to the S-doping strategy and the choice of the current TEG device structure.

Finally, a self-powered motion detector can be realized by the current optimized S-doped Ag_2Se TEG through harvesting the ΔT between a human body (e.g. human hand) and an ambient temperature (e.g. at ~20-25 °C). As shown in Fig. 6(c) and (d), when the TEG was held in hand with its hot end contacting the palm and its cold end remaining in air, an infrared camera reveals that the temperature of the hand can reach ~ 31 °C, while that of the cold end stayed at ~ 25 °C (Fig. 6(d), measured at the 'green-cross' location with the measured value shown at the upper left corner of the image), leading to a ΔT of typically in the range of 4-6 K. While such a ΔT is not large, by which the TEG can generate an opencircuit voltage of ~6-7 mV (Fig. 6(c)). As a proof of concept, the output of the TEG was connected to a simple circuit with two resistors connected in series (Fig. 6(g)), among which one is a fixedvalue resistor ($R_{1(fixed)}$ = 1.19 MΩ) and the other one is a force (f)-sensing variable resistor (R_f) which was attached to the arm. Due to the drastic decrease of the R_f value during the arm movements (i.e. R_f (f = 0 kg) ~ 59 MΩ decreased to R_f (f = ~1 kg) ~ 2 kΩ)), the part of the output voltage (provided by the hand-held TEG) felt onto R_1 can be read out and associated with arm movements (Fig. 6(h), video available in supplementary information). As a result, the combination of the hand-held TEG based on S-doped Ag_2Se together with the above-mentioned circuit provided self-powered human motion detection with a sensitivity of ~6 mV/kg (or ~ 0.3 μV/Pa) in terms of voltage readout per unit of force. This sensitivity is within the same order of magnitude as compared to the previous flexible TEGs applying 25 pairs of Bi_2Te_3/Sb_2Te_3 legs sputtered on polyimide substrates, where a sensitivity of ~0.6 μV/Pa was obtained under a ΔT of 5 K [56]. For the similar type of arm movements, the current voltage peak-to-peak readout (~6 mV) is significantly higher than that reported previously on fibers-based TEGs (~0.2 mV) [57]. We expect that the present sensitivity can be further increased by engineering means such as the application of a more sensitive R_f and/

or a Wheatstone bridge-type circuit. Indeed, other TE materials than the current S-doped Ag_2Se system can possibly also achieve the above-mentioned applications. But the combined advantages of the current system in terms of low synthesis temperature, mechanical flexibility, high power density, and absence of toxic heavymetal elements render it particularly attractive in this regard.

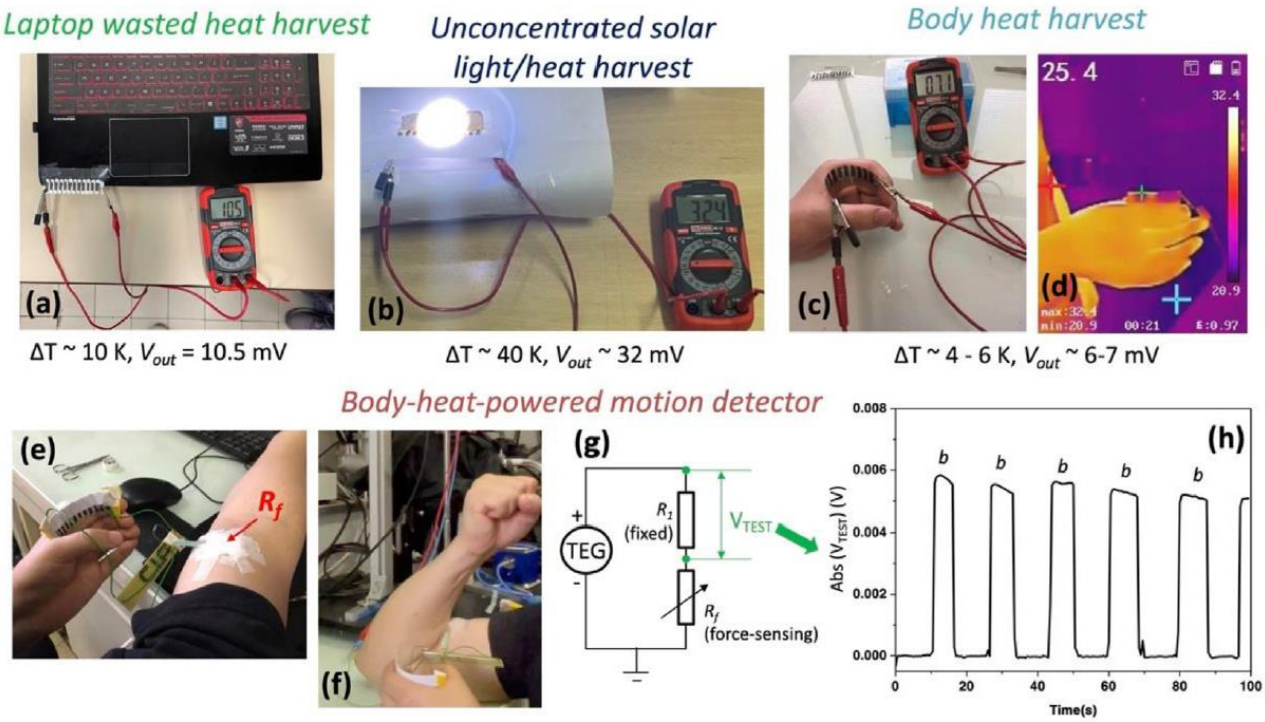

Fig. 6. Different demonstrations applying the optimized flexible S-doped Ag2Se thermoelectric generator (TEG) to harvest near-room temperature low-grade heat. (a)-(c) The harvest of a laptop waste heat (a), or non-concentrated (simulated) 1-sun illumination (b), or human body (hand) (c). For the application in (b), a photothermal Au NP coating (which converts the sun illumination to heat) was applied onto the hot end of the TEG, while the cold end of the TEG was covered, preventing direct sun-light-heating. The ΔT achieved in (a), (b), and (c) was respectively from the temperature difference between the laptop (a), or the photothermal Au NP coating (b), or the hand (c) and the cold end of the TEG kept under ambient conditions. (d) Exhibits the infrared image confirming the ΔT in (c). The measured temperature at the location of the green-cross (at the cold end of the device) is shown at the upper left corner of the image (25.4 °C). The red and blue cross represent, respectively, the highest and lowest temperature point of the image (measured value shown in the scale bar). (e)-(h) By harvesting the body heat, the TEG can be further applied to detect motion by connecting its output to two resistors in series, R_1 (fixed) = 1.19 MΩ and R_f (a force-sensing variable resistor) which is attached to arm ((e) and (f), circuit shown in (g)). (h) The evolution of the voltage felt onto R_1 over time when the arm was bent multiple times (corresponding voltage peaks labeled as 'b').

4. Conclusions

In summary, a new RT one-pot solution synthesis approach was proposed to achieve and deposit functional n-type flexible Ag_2Se TE thin films with the necessity of only a mild post-deposition heattreatment at 150 °C. The sulfur-doping strategy was investigated here, leading to an optimization on both the flexibility and the TE characteristics of the achieved TE thin films. The most optimized S-doped Ag_2Se thin films exhibited a maximum *PF* of ~2058 μW/m/K at RT and maintained >90% of their initial *PF* after 1000 cycles of bending with a bending radius of 6 mm. Flexible TEGs, capable of performing near-RT energy harvest, were then fabricated, allowing for a maximum power output P_{max} of 3.98 μW and a maximum power density $P_{density}$ of 11.06 W/m^2 at ΔT = ~30 K near RT. Multidomain demonstrations were made to apply these flexible Sdoped Ag_2Se TEGs to harvest low-grade heat from a laptop computer, the non-concentrated sun light, and the human body together with the realization of a TEG-enabled self-powered human motion detector exhibiting a sensitivity of 6 mV/kg in terms of voltage readout per unit of force. The current functional and flexible S-doped Ag_2Se TEGs, free of heavy-metal elements and achieved by a solution

synthesis compatible to scalable deposition methods, thus provide exciting perspectives for the ongoing development of wearable smart electronics and energy harvesting.

Credit author statement

C. Xin: methodology, investigation, synthesis, data acquisition, formal analysis, and writing e original draft. S. Jiang: measurements by the PPMS setup. Z. Hu: EDX measurements. D. Zhang: TEG characterizations. Z. Fang: SEM/EDX , XRD, and TEG characterizations. F. Cassagne: circuit building for TEG characterizations. L. Aigouy: assistance in data analysis and manuscript writing. Z. Chen: conceptualization, supervision, funding acquisition, editing, review, and submission.

Declaration of competing interest

The authors declare that they have no known competing financial interests or personal relationships that could have appeared to influence the work reported in this paper.

Data availability

Data will be made available on request.

Acknowledgments

This work is supported by the recurring laboratory funding from CNRS and ESPCI Paris. We thank Dr Kamran Behnia and Dr. Benoît Fauque (both from LPEM, ESPCI Paris/CNRS) for valuable discussions and assistance in experiments related to the PPMS setup. We thank Mr. Bruno Bresson (from SIMM laboratory, ESPCI Paris/CNRS) for assistance related to the SEM/EDX measurements. C. Xin, D. Zhang, and Z. Fang acknowledge the China Scholarship Council (CSC) for their PhD scholarships.

Appendix A. Supplementary data

Supplementary data to this article can be found online at https://doi.org/10.1016/j.mtener.2023.101266.

References

[1] J.H. Bahk, H. Fang, K. Yazawa, A. Shakouri, Flexible thermoelectric materials and device optimization for wearable energy harvesting, J Mater Chem C Mater 3 (2015) 10362-10374, https://doi.org/10.1039/c5tc01644d.

[2] L. Zhang, S. Lin, T. Hua, B. Huang, S. Liu, X. Tao, Fiber-based thermoelectric generators: materials, device structures, fabrication, characterization, and applications, Adv. Energy Mater. 8 (2018), 1700524, https://doi.org/10.1002/ aenm.201700524.

[3] O. Bubnova, X. Crispin, Towards polymer-based organic thermoelectric generators, Energy Environ. Sci. 5 (2012) 9345, https://doi.org/10.1039/ c2ee22777k.

[4] S. Khan, J. Kim, S. Acharya, W. Kim, Review on the operation of wearable sensors through body heat harvesting based on thermoelectric devices, Appl. Phys. Lett. 118 (2021), 200501, https://doi.org/10.1063/5.0049347.

[5] Y. Mona, T.A. Do, C. Sekine, P. Suttakul, C. Chaichana, Geothermal electricity generator using thermoelectric module for IoT monitoring, Energy Rep. 8 (2022) 347-352, https://doi.org/10.1016/j.egyr.2022.02.114.

[6] T.T. Kim Tuoi, N. van Toan, T. Ono, Heat storage thermoelectric generator for wireless IOT sensing systems, in: 2021 21st International Conference on SolidState Sensors, Actuators and Microsystems (Transducers), IEEE, 2021, pp. 924-927, https://doi.org/10.1109/Transducers50396.2021.9495686.

[7] Q. Yang, S. Yang, P. Qiu, L. Peng, T.-R. Wei, Z. Zhang, X. Shi, L. Chen, Flexible thermoelectrics based on ductile semiconductors, Science 377 (2022) 854-858, https://doi.org/10.1126/science.abq0682.

[8] Y. Xiong, G. Zhou, N.-C. Lai, X. Wang, Y.-C. Lu, O.v. Prezhdo, D. Xu, Chemically switchable n-type and p-type conduction in bismuth selenide nanoribbons for thermoelectric energy harvesting, ACS Nano 15 (2021) 2791-2799, https:// doi.org/10.1021/acsnano.0c08685.

[9] Y. Han, J. Zhang, R. Hu, D. Xu, High-thermopower polarized electrolytes enabled by methylcellulose for low-grade heat harvesting, Sci. Adv. 8 (2022), https://doi.org/10.1126/sciadv.abl5318.

[10] S. Hong, Y. Gu, J.K. Seo, J. Wang, P. Liu, Y.S. Meng, S. Xu, R. Chen, Wearable thermoelectrics for personalized thermoregulation, Sci. Adv. 5 (2019), https:// doi.org/10.1126/sciadv.aaw0536.

[11] J. Zang, J. Chen, Z. Chen, Y. Li, J. Zhang, T. Song, B. Sun, Printed flexible thermoelectric materials and devices, J Mater Chem A Mater 9 (2021) 19439-19464, https://doi.org/10.1039/D1TA03647E.

[12] L. Wang, J. Zhang, Y. Guo, X. Chen, X. Jin, Q. Yang, K. Zhang, S. Wang, Y. Qiu, Fabrication of core-shell structured poly(3,4-ethylenedioxythiophene)/carbon nanotube hybrid with enhanced thermoelectric power factors, Carbon N Y 148 (2019) 290-296, https://doi.org/10.1016/j.carbon.2019.03.088.

[13] T. Luo, K. Pan, Flexible thermoelectric device based on poly(ether- b-amide 12) and high-purity carbon nanotubes mixed bilayer heterogeneous films, ACS Appl. Energy Mater. 1 (2018) 1904-1912, https://doi.org/10.1021/ acsaem.7b00190.

[14] H. Wang, X. Liu, Z. Zhou, H. Wu, Y. Chen, B. Zhang, G. Wang, X. Zhou, G. Han, Constructing n-type Ag2Se/CNTs composites toward synergistically enhanced thermoelectric and mechanical performance, Acta Mater. 223 (2022), 117502, https://doi.org/10.1016/j.actamat.2021.117502.

[15] T. Varghese, C. Dun, N. Kempf, M. Saeidi-Javash, C. Karthik, J. Richardson, C. Hollar, D. Estrada, Y. Zhang, Flexible thermoelectric devices of ultrahigh power factor by scalable printing and interface engineering, Adv. Funct. Mater. 30 (2020) 1-8, https://doi.org/10.1002/adfm.201905796.

[16] J. Liang, T. Wang, P. Qiu, S. Yang, C. Ming, H. Chen, Q. Song, K. Zhao, T.R. Wei, D. Ren, Y.Y. Sun, X. Shi, J. He, L. Chen, Flexible thermoelectrics: from silver chalcogenides to full-inorganic devices, Energy Environ. Sci. 12 (2019) 2983-2990, https://doi.org/10.1039/c9ee01777a.

[17] S. He, Y. Li, L. Liu, Y. Jiang, J. Feng, W. Zhu, J. Zhang, Z. Dong, Y. Deng, J. Luo, W. Zhang, G. Chen, Semiconductor glass with superior flexibility and high room temperature thermoelectric performance, Sci. Adv. 6 (2020) 1-8, https://doi.org/10.1126/sciadv.aaz8423.

[18] Y. Ding, Y. Qiu, K. Cai, Q. Yao, S. Chen, L. Chen, J. He, High performance n-type Ag 2 Se film on nylon membrane for flexible thermoelectric power generator, Nat. Commun. 10 (2019) 1-7, https://doi.org/10.1038/s41467-019-08835-5.

[19] M. Wu, K. Cai, X. Li, Y. Li, Y. Liu, Y. Lu, Z. Wang, W. Zhao, P. Wei, Ultraflexible and high-thermoelectric-performance sulfur-doped Ag 2 Se film on nylon for power generators, ACS Appl. Mater. Interfaces 14 (2022) 4307-4315, https:// doi.org/10.1021/acsami.1c21701.

[20] X. Li, Y. Lu, K. Cai, M. Gao, Y. Li, Z. Wang, M. Wu, P. Wei, W. Zhao, Y. Du, S. Shen, Exceptional power factor of flexible Ag/Ag2Se thermoelectric composite films, Chem. Eng. J. 434 (2022), 134739, https://doi.org/10.1016/j.cej.2022.134739.

[21] S. Acharya, B. Yu, J. Hwang, J. Kim, W. Kim, High thermoelectric performance of ZnO by coherent phonon scattering and optimized charge transport, Adv. Funct. Mater. 31 (2021), 2105008, https://doi.org/10.1002/adfm.202105008.

[22] Y. Zhao, L. Liu, F. Zhang, C. Di, D. Zhu, Advances in organic thermoelectric materials and devices for smart applications, SmartMat 2 (2021) 426-445, https://doi.org/10.1002/smm2.1034.

[23] O. Bubnova, Z.U. Khan, A. Malti, S. Braun, M. Fahlman, M. Berggren, X. Crispin, Optimization of the thermoelectric figure of merit in the conducting polymer poly(3,4-ethylenedioxythiophene), Nat. Mater. 10 (2011) 429-433, https:// doi.org/10.1038/nmat3012.

[24] Q. Zhang, Y. Sun, W. Xu, D. Zhu, Organic thermoelectric materials: emerging green energy materials converting heat to electricity directly and efficiently, Adv. Mater. 26 (2014) 6829e6851, https://doi.org/10.1002/adma.201305371.

[25] G.H. Kim, L. Shao, K. Zhang, K.P. Pipe, Engineered doping of organic semiconductors for enhanced thermoelectric efficiency, Nat. Mater. 12 (2013) 719-723, https://doi.org/10.1038/nmat3635.

[26] T. Park, C. Park, B. Kim, H. Shin, E. Kim, Flexible PEDOT electrodes with large thermoelectric power factors to generate electricity by the touch of fingertips, Energy Environ. Sci. 6 (2013) 788, https://doi.org/10.1039/c3ee23729j.

[27] B. Meng, J. Liu, L. Wang, Recent development of n-type thermoelectric materials based on conjugated polymers, Nano Materials Science 3 (2021) 113-123, https://doi.org/10.1016/j.nanoms.2020.10.002.

[28] J. Li, A.B. Huckleby, M. Zhang, Polymer-based thermoelectric materials: areview of power factor improving strategies, J Materiomic 8 (2022) 204-220, https://doi.org/10.1016/j.jmat.2021.03.013.

[29] W. Zhou, Q. Fan, Q. Zhang, L. Cai, K. Li, X. Gu, F. Yang, N. Zhang, Y. Wang, H. Liu, W. Zhou, S. Xie, High-performance and compact-designed flexible thermoelectric modules enabled by a reticulate carbon nanotube architecture, Nat. Commun. 8 (2017), 14886, https://doi.org/10.1038/ncomms14886.

[30] M. Ferhat, J. Nagao, Thermoelectric and transport properties of b-Ag2Se compounds, J. Appl. Phys. 88 (2000) 813-816, https://doi.org/10.1063/ 1.373741.

[31] J. Capps, F. Drymiotis, S. Lindsey, T.M. Tritt, Significant enhancement of the dimensionless thermoelectric figure of merit of the binary Ag 2 Te, Phil. Mag. Lett. 90 (2010) 677-681, https://doi.org/10.1080/09500839.2010.495355.

[32] F.F. Aliev, M.B. Jafarov, V.I. Eminova, Thermoelectric figure of merit of Ag2Se with Ag and Se excess, Semiconductors 43 (2009) 977-979, https://doi.org/ 10.1134/S1063782609080028.

[33] X. Shi, H. Chen, F. Hao, R. Liu, T. Wang, P. Qiu, U. Burkhardt, Y. Grin, L. Chen, Room-temperature ductile inorganic semiconductor, Nat. Mater. 17 (2018) 421-426, https://doi.org/10.1038/s41563-018-0047-z.

[34] J.A. Perez-Taborda, O. Caballero-Calero, L. Vera-Londono, F. Briones, M. Martin-Gonzalez, High thermoelectric zT in n-type silver selenide films at room temperature, Adv. Energy Mater. 8 (2018), 1702024, https://doi.org/ 10.1002/aenm.201702024.

[35] R. Sadanaga, S. Sueno, X-RAY STUDY ON THE ^|^alpha;-^|^beta; TRANSITION OF Ag2S, Mineral. J. 5 (1967) 124-143, https://doi.org/10.2465/minerj1953.5. 124.

[36] M.M. Mallick, A.G. Rosch, L. Franke, A. Gall, S. Ahmad, H. Geßwein, A. Mazilkin, € C. Kübel, U. Lemmer, New frontier in printed thermoelectrics: formation of bAg2Se through thermally stimulated dissociative adsorption leads to high: ZT, J Mater Chem A Mater 8 (2020) 16366-16375, https://doi.org/10.1039/ d0ta05859a.

[37] J.-Y. Kim, W. Lee, Y.H. Kang, S.Y. Cho, K.-S. Jang, Wet-spinning and posttreatment of CNT/PEDOT:PSS composites for use in organic fiber-based thermoelectric generators, Carbon N Y 133 (2018) 293-299, https://doi.org/ 10.1016/j.carbon.2018.03.041.

[38] C.T. Hong, Y.H. Kang, J. Ryu, S.Y. Cho, K.-S. Jang, Spray-printed CNT/P3HT organic thermoelectric films and power generators, J Mater Chem A Mater 3 (2015) 21428-21433, https://doi.org/10.1039/C5TA06096F.

[39] Y. Lu, Y. Qiu, K. Cai, Y. Ding, M. Wang, C. Jiang, Q. Yao, C. Huang, L. Chen, J. He, Ultrahigh power factor and flexible silver selenide-based composite film for thermoelectric devices, Energy Environ. Sci. 13 (2020) 1240-1249, https:// doi.org/10.1039/c9ee01609k.

[40] C. Xin, Z. Hu, Z. Fang, M. Chaudhary, H. Xiang, X. Xu, L. Aigouy, Z. Chen, Flexible and wearable plasmonic-enabled organic/inorganic hybrid photothermoelectric generators, Mater. Today Energy 22 (2021), 100859, https:// doi.org/10.1016/j.mtener.2021.100859.

[41] J. Xie, M. Han, X. Zeng, D. Mao, H. Li, X. Zeng, R. Liu, L. Ren, R. Sun, J. Xu, Flexible pCu2Se-nAg2Se thermoelectric devices via in situ conversion from printed Cu patterns, Chem. Eng. J. 435 (2022), 135172, https://doi.org/ 10.1016/j.cej.2022.135172.

[42] A. Sahu, L. Qi, M.S. Kang, D. Deng, D.J. Norris, Facile synthesis of silver chalcogenide (Ag 2 E; E ¼ Se, S, Te) semiconductor nanocrystals, J. Am. Chem. Soc. 133 (2011) 6509-6512, https://doi.org/10.1021/ja200012e.

[43] T. Bai, C. Li, F. Li, L. Zhao, Z. Wang, H. Huang, C. Chen, Y. Han, Z. Shi, S. Feng, A simple solution-phase approach to synthesize high quality ternary AgInSe2 and band gap tunable quaternary AgIn(S1xSex)2 nanocrystals, Nanoscale 6 (2014) 6782, https://doi.org/10.1039/c4nr00233d.

[44] C. Wang, Y. Wang, L. Xu, D. Zhang, M. Liu, X. Li, H. Sun, Q. Lin, B. Yang, Facile aqueous-phase synthesis of biocompatible and fluorescent Ag 2 S nanoclusters for bioimaging: tunable photoluminescence from red to near infrared, Small 8 (2012) 3137-3142, https://doi.org/10.1002/smll.201200376.

[45] S. Tang, C. He, D. Li, W. Cai, L. Fan, Y. Li, Precursor reactivity differentiation for single-step preparation of Ag2Se@Ag2S coreeshell nanocrystals with distinct absorption and emission properties enabling sensitive near-infrared photodetection, J. Mater. Sci. 53 (2018) 11355e11366, https://doi.org/10.1007/ s10853-018-2465-3.

[46] W. Yang, S. Mao, J. Yang, T. Shang, H. Song, J. Mabon, W. Swiech, J.R. Vance, Z. Yue, S.J. Dillon, H. Xu, B. Xu, Large-deformation and high-strength amorphous porous carbon nanospheres, Sci. Rep. 6 (2016), 24187, https://doi.org/ 10.1038/srep24187.

[47] L.L. Baranowski, G. Jeffrey Snyder, E.S. Toberer, Response to “Comment on ‘Effective thermal conductivity in thermoelectric materials’” [J. Appl. Phys. 113, 204904 (2013)], J. Appl. Phys. 115 (2014), 126102, https://doi.org/10.1063/ 1.4869140.

[48] A. Montecucco, J. Siviter, A.R. Knox, Constant heat characterisation and geometrical optimisation of thermoelectric generators, Appl. Energy 149 (2015) 248e258, https://doi.org/10.1016/j.apenergy.2015.03.120.

[49] Y. Lu, Y. Qiu, K. Cai, X. Li, M. Gao, C. Jiang, J. He, Ultrahigh performance PEDOT/ Ag2Se/CuAgSe composite film for wearable thermoelectric power generators, Mater Today Phy 14 (2020), https://doi.org/10.1016/j.mtphys.2020.100223.

[50] Y. Lu, Y. Ding, Y. Qiu, K. Cai, Q. Yao, H. Song, L. Tong, J. He, L. Chen, Good performance and flexible PEDOT:PSS/Cu 2 Se nanowire thermoelectric composite films, ACS Appl. Mater. Interfaces 11 (2019) 12819-12829, https:// doi.org/10.1021/acsami.9b01718.

[51] Q. Xu, S. Qu, C. Ming, P. Qiu, Q. Yao, C. Zhu, T.R. Wei, J. He, X. Shi, L. Chen, Conformal organic-inorganic semiconductor composites for flexible thermoelectrics, Energy Environ. Sci. 13 (2020) 511-518, https://doi.org/10.1039/ c9ee03776d.

[52] D. Ni, H. Song, Y. Chen, K. Cai, Free-standing highly conducting PEDOT films for flexible thermoelectric generator, Energy 170 (2019) 53-61, https:// doi.org/10.1016/j.energy.2018.12.124.

[53] Z. Wang, Q. Gao, W. Wang, Y. Lu, K. Cai, Y. Li, M. Wu, J. He, High performance Ag2Se/Ag/PEDOT composite films for wearable thermoelectric power generators, Mater Today Phy 21 (2021), https://doi.org/10.1016/j.mtphys.2021. 100553, 0e5.

[54] M. Sheng, Y. Wang, C. Liu, Y. Xiao, P. Zhu, Y. Deng, Significantly enhanced thermoelectric performance in SWCNT films via carrier tuning for high power generation, Carbon N Y 158 (2020) 802-807, https://doi.org/10.1016/ j.carbon.2019.11.057.

[55] Y. Jia, Q. Jiang, H. Sun, P. Liu, D. Hu, Y. Pei, W. Liu, X. Crispin, S. Fabiano, Y. Ma, Y. Cao, Wearable thermoelectric materials and devices for self-powered electronic systems, Adv. Mater. 33 (2021), 2102990, https://doi.org/10.1002/ adma.202102990.

[56] Y. Wang, W. Zhu, Y. Deng, B. Fu, P. Zhu, Y. Yu, J. Li, J. Guo, Self-powered wearable pressure sensing system for continuous healthcare monitoring enabled by flexible thin-film thermoelectric generator, Nano Energy 73 (2020), 104773, https://doi.org/10.1016/j.nanoen.2020.104773.

[57] T. Sun, B. Zhou, Q. Zheng, L. Wang, W. Jiang, G.J. Snyder, Stretchable fabric generates electric power from woven thermoelectric fibers, Nat. Commun. 11 (2020) 572, https://doi.org/10.1038/s41467-020-14399-6.